

MICROSTRUCTURE AND TENSILE PROPERTIES OF ALUMINUM MATRIX COMPOSITES REINFORCED WITH SiC NANOPARTICLES COATED GRAPHENE

H. T. QI^a, J. B. GAO^b, K. F. ZHENG^a, X. M. DU^{*a}, F. G. LIU^a

^a School of Materials Science and Engineering, Shenyang Ligong University, Shenyang 110159, China.

^b Centre of Excellence for Advanced Materials, Dongguan 523808, China.

In this paper, the composite reinforced phases that SiC nanoparticles were coated with graphene were prepared by high energy ball milling. The coated situation and strengthening effect of two kinds of reinforced phases with different proportion were investigated. XRD, SEM and TEM were used to characterize composite powders and composite samples. It was found that the microstructure of graphene was destroyed with the increase of the ratio of graphene vs SiC nanoparticle. In addition, the reinforced phase in the samples of all composite materials is mainly distributed at the Al grain boundaries. The ultimate tensile strength (UTS) of the composite with the ratio of the two reinforced phases was 1:1 reached the maximum value, which was 44.63% higher than that of the matrix. The fracture mechanism of the composites changed from toughness to brittleness with the increase of the ratio of the two reinforced phases.

(Received December 13, 2019; Accepted May 4, 2020)

Keywords: Graphene, SiC nanoparticle, Aluminum matrix composite, Tensile properties

1. Introduction

Aluminum matrix composites (AMC) have been investigated since 1920 because of their excellent mechanical and physical properties[1,2]. And because of its lightweight characteristics, it is widely used in many industrial fields, such as electronic packaging, armours and automotive. [3-5]. Nowadays, aluminum (Al) has been widely used second only to iron in the world, indicating that aluminum matrix composites have great application space[6]. Graphene is a kind of two-dimensional honeycomb crystal structure nanomaterials composed of carbon atoms[7]. In recent years, it has attracted a lot of attention owing to its outstanding mechanical, conductive and other physical properties[8]. Up to now, researchers have carried out research in many aspects, such as graphene/metal matrix, graphene/ceramic composites and so on[9-14]. Even if trying to disperse graphene uniformly into metal matrix composites by high energy ball milling, electrostatic self-assembly and so on[15,16], the research results are not ideal due to the characteristics of large specific surface area and easy agglomeration of graphene. Many researchers tried to improve the dispersion effect by adding ceramic particles. The addition of ceramic particles is helpful to the dispersion of graphene, but it will also cause different degrees of

*Corresponding author: du511@163.com

stress concentration on the matrix, because the morphology of ceramic particles is polygonal[17]. This brings another kind of harm to the properties of the composites.

In this study, a new method was proposed for the problem of hybrid reinforced metal matrix composites of graphene and ceramic particles (SiC nanoparticles used in this study) using SiC nanoparticles coated with graphene to form core-shell structure and sandwich structure to avoid direct contact between ceramic particles and the matrix. According to this method, the composite effects of different ratios of graphene/SiC nanoparticles were investigated, and the composite samples were prepared. The microstructure and mechanical properties of the composites with different ratios of graphene/SiC nanoparticles were also studied.

2. Experimental details

2.1. Preparation of composites

Graphene used in this study is provided by Nanjing XFNANO material Technology Co., Ltd., with a diameter of 5-10 μm and a thickness of 3-10 nm. SiC nanoparticles are provided by Shanghai Yunfu Nanotechnology Co., Ltd., with a particle size of 800 nm. The composite particles were prepared by planetary high energy ball milling. The zirconia grinding ball with a diameter of 10 mm was selected as the grinding medium. The mass ratio of grinding ball to composite powder is 15: 1. The rotational speed is 300rpm. The time is 3hours. A schematic diagram of the preparation of composite particles is shown in Fig. 1. Different ratios of graphene vs SiC nanoparticles (1: 1, 1: 2, 1: 3, 1: 4) were placed in the ball milling container, and the grinding ball with larger diameter was selected to improve the impact force in the process of ball milling. The resulting core-shell structure and sandwich structure are shown in Fig. 1.

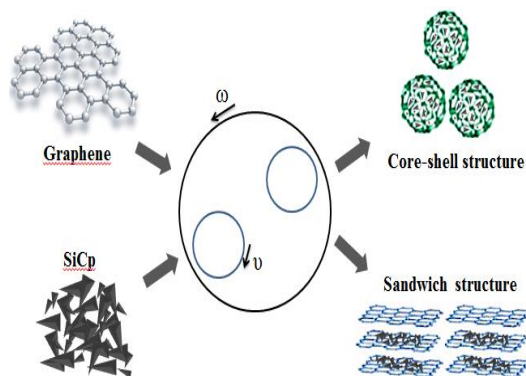


Fig. 1. Schematic diagram of preparation of composite powder.

The content of graphene in the composite samples to be prepared is 0.25wt.%, and the content of SiC nanoparticles is 0.25, 0.5, 0.75 and 1.0 wt.% (1: 1, 1: 2, 1: 3, 1: 4), respectively. Then the prepared composite powders and Al7075(Al-Zn-Mg-Cu alloy) alloy powder(10 μm , supplied from Beijing Hongyu Materials Company) are subjected to secondary high energy ball milling. The mass ratio of grinding ball to powder was 5: 1. The rotational speed and time of ball milling was the same to the aforementioned ball-milling. For every hour of high energy ball milling, it needs to be paused for 15 minutes to prevent the aluminum alloy powder from overheating.

The uniformly mixed composite powder is placed in a heat-resistant steel mold (diameter 50 mm, height 200 mm, thickness 10 mm) to be suppressed using vacuum hot-press sintering furnace (ZR-6-8Y, Shanghai Chenhua Electric Furnace Co., Ltd., Shanghai). The composite powders were consolidated in vacuum hot press at 610°C for 3 hours under a pressure of 30 MPa using graphite paper as lubricants between the punch and die walls. For comparison, a pure Al7075 alloy sample was also prepared under the same conditions. The composite samples were treated by solid solution treatment at 470 °C for 2 h, and quenched with cold water. Then artificial aging was carried out at 140 °C for 16 h.

2.2. Characterization of composites

The morphology of composite powders with different ratios of graphene vs SiC nanoparticles was observed by scanning electron microscope (Hitachi S-3400, Japan). The microstructure of the composite samples was observed by scanning electron microscope (SEM, TESCAN) with energy dispersive spectroscopy (EDS). The samples for DF-STEM observations were first mechanically polished into thin foils of 80µm and then electro-polished using a twin double jet system in a solution of 33% nitric acid in methanol at -20°C and 15V. The observations were performed in a JEOL-TEM 200F equipped with a Schottky field emitter and operating at 200kV. X-ray diffraction analysis on polished samples were carried out by X-ray diffraction (Rigaku Ultima IV), using Cu K_α radiation in the range of 2θ-40 degrees and 2θ-100 degrees for composite powders and the sintered composite samples, respectively. Raw XRD data were refined and analyzed via MDI Jade 6.0 program (Materials Data Incorporated: Livermore, CA, USA).

The Vickers hardness of the sample was measured using a Vickers hardness tester (HVS-50, Shanghai, China). The load force is set to 9.8 N and the dwell time is 10 s. The average hardness of the material is measured at least 5 times in different areas of each sample. Normalized tensile specimens with a gauge length of 15 mm, a gauge width of 3 mm and a thickness of 2 mm were used. The ultimate tensile strength (UTS) was measured using a computerized universal testing machine (UTM4304, Shenzhen Suns Technology Stock Co., Ltd, China) at a cross head speed of 0.5 mm/s. The fracture surfaces of the failed tensile specimens were observed using SEM.

3. Results and discussion

Fig. 2 shows the micro-morphology of the composite powders with different ratio of graphene vs SiC nanoparticles after 3 hours high-energy ball milling. It can be found that almost no SiC nanoparticles are separate from graphene sheets for the composite powders with ratio of 1:1. SiC nanoparticles embedded in graphene sheets. The graphene sheets exhibit a curled state. When the ratio is 1:2, a part of the SiC nanoparticles are separate from the graphene, and the rest part of the SiC nanoparticles are adhered to the surface of the graphene. The morphology of the graphene was not clearly observed. The desired coating is not achieved. It can be observed that a large amount of SiC nanoparticles are aggregated on the surface of graphene to form agglomerated clusters for 1:3 of the ratio. Many SiC nanoparticles are still separate. Continue to increase the proportion to 1:4, the size of the graphene particles is greatly reduced. The SiC nanoparticles are wrapped on the outside of the graphene and a large amount of SiC nanoparticles are separate. It shows that the ratio of 1:1 is a suitable ratio for graphene vs SiC nanoparticles.

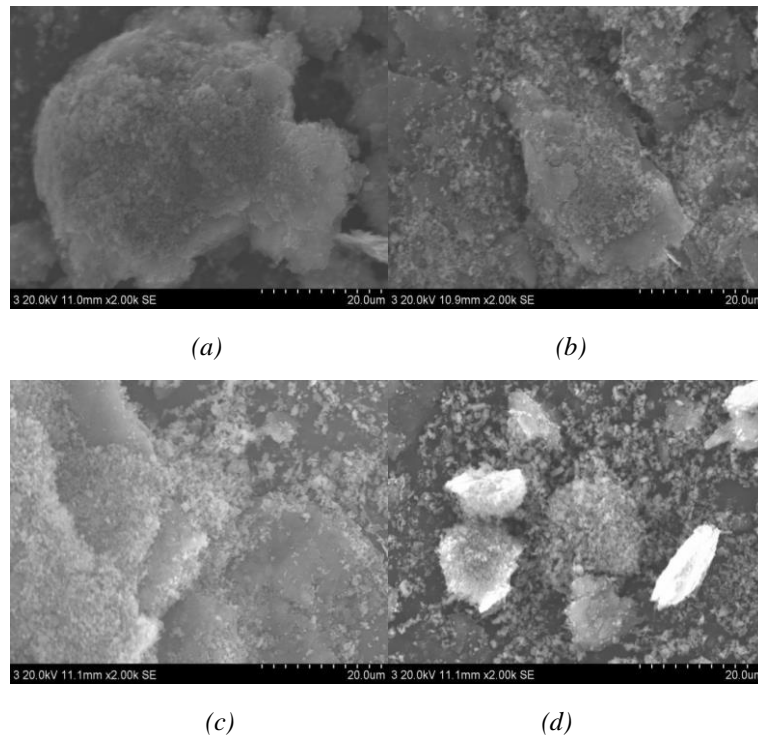


Fig. 3. Microscopic morphology of composite powder with different composite proportion
(a)1:1,(b)1:2,(c)1:3,(d)1:4.

Fig. 4 shows the X-ray diffraction pattern of the four composite powders. It is easy to find that the X-ray diffraction peak intensity of graphene decreases and broadens obviously with the increase of the ratio of graphene vs SiC nanoparticles. However, the diffraction peak of SiC has no obvious change. This shows that the increase of the content of the SiC nanoparticles leads to the more lattice defects and the destruction of the structure in graphene. This is because the shear interaction between SiC nanoparticles and graphene destructs the structure of graphene in the process of high energy ball milling, which reduces the order of structure in graphene and leads to the broadening of diffraction peak.

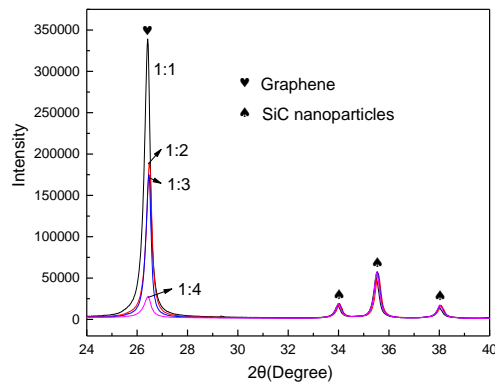


Fig. 4. X-ray diffraction pattern of composite powders in different proportions.

Fig. 5 showed the microstructure of aluminum matrix composites containing different ratios of composite powders. Seen from Fig. 5a, a very clear grain boundary can be observed. A high content of C element was detected at the boundary by EDS, indicating that the reinforced phases are distributed at the grain boundary. Graphenes with wrinkled surfaces on which were clearly observed and a few SiC nanoparticles were separate nearby in Fig. 5b. These reinforced phases mainly distributed at the grain boundary. The large content of C element at the grain boundary was also found in the EDS from Fig. 5c. No obvious graphene was found. Only a large number of SiC nanoparticles were found at the grain boundary in Fig. 5d. To sum up, the graphene-SiC nanoparticles composite reinforced phases were mainly distributed at the grain boundary. And the number of dispersed SiC nanoparticles increases with the increase of the ratio of the two strengthening phases.

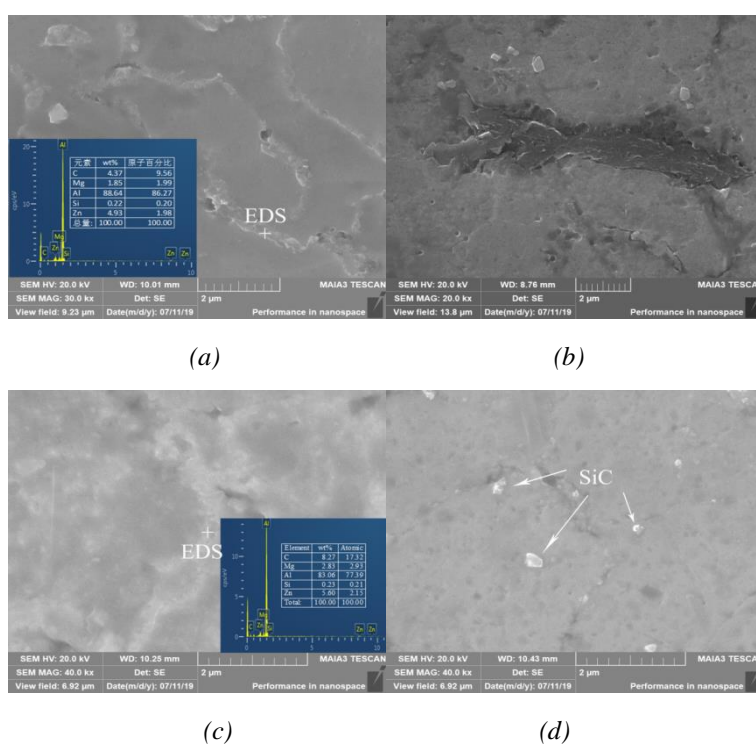


Fig. 5. Microstructure of aluminum matrix composites containing different ratios of composite powders (a)1:1,(b)1:2,(c)1:3,(d)1:4.

As shown in Fig. 6, the TEM microscopic picture and EDS results of the aluminum matrix composite sample with the ratio of 1:1 for graphene vs SiC nanoparticles. In Fig. 6a, the black part that can be observed is graphene. It can be verified from Fig. 6c, in which the content of carbon element is high and the distribution of carbon element is consistent with morphology in Fig. 6a. Moreover, graphene can be also seen to be bonded to the matrix. No Al_4C_3 was found at the interface between graphenes and aluminum matrices. Al_4C_3 was clearly observed on the bonding interface between carbon nanotubes and aluminum matrices for carbon nanotube reinforced Al2024 composites under TEM[18]. The morphology of Al_4C_3 in graphene reinforced Al5083 composites [19] was the same as that reported in Ref.[18]. It is worth noting that there are a large number of Si elements in the graphene region through the detection results of EDS (Fig. 6d). This

indicates that SiC nanoparticles and graphene coexist in Fig. 6a and SiC nanoparticles were successfully wrapped in graphene.

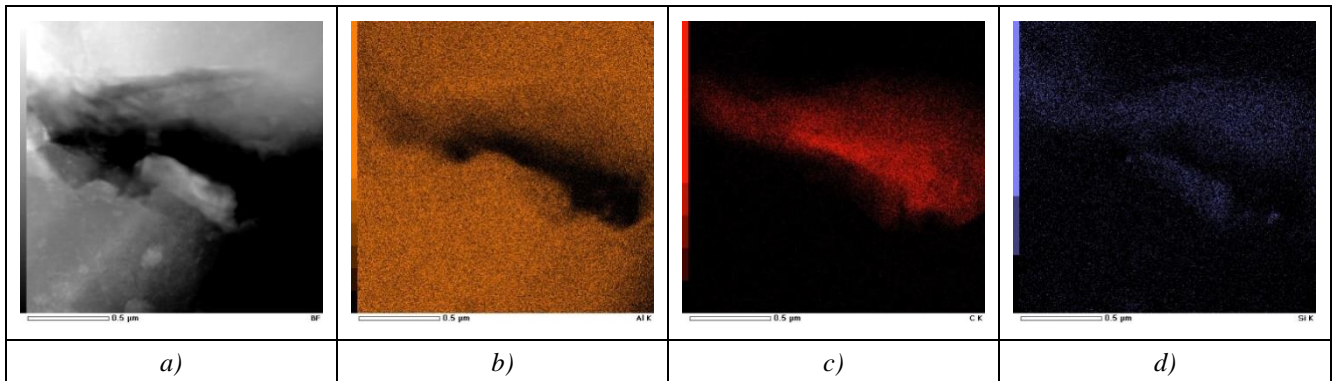


Fig. 6. TEM micrographs and EDS results of aluminum matrix composite samples with ratios of 1:1 for graphene vs SiC nanoparticles, (a)TEM,(b) Mapping of Al in EDS,(c) Mapping of C in EDS,(d) Mapping of Si in EDS.

The X-ray diffraction pattern of aluminum matrix composites after vacuum hot pressing is shown in Fig.7. The diffraction peaks of Al, SiC, MgZn₂ and Al₂CuMg were detected in the diffraction patterns. Due to the detection limit of XRD, graphene and SiC with low content in the composites were not detected. The diffraction peak of SiC was found in the aluminum matrix composite sample with a composite powder ratio of 1:3 and 1:4 at 35.65°. In addition, aluminum carbide was not found in the X-ray diffraction patterns of all composite samples. In the report of Bustamante et al. [20], the formation of aluminum carbide is closely related to the processing temperature set in the preparation of the composites.

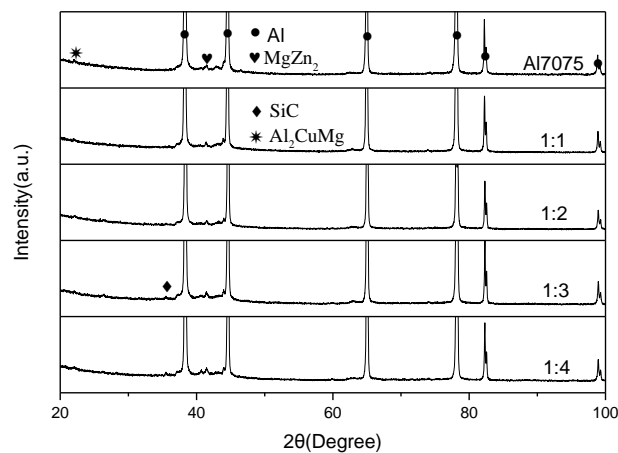


Fig. 7. X-ray diffraction pattern of aluminum matrix composites.

Fig. 8 shows the Vickers hardness of aluminum matrix composites containing different ratios of composite powders. It can be found that the hardness of those composite samples is

significantly higher than that of the pure Al7075 sample, which increases by 17.37%, 24.20%, 24.87% and 25.87%, respectively. And with the increase of the ratio of composite powder, the hardness increases. Compared with the matrix, the strengthening of the composite is mainly due to the following reasons: (1) the thermal mismatch caused by the different coefficient of thermal expansion (CTE) between the reinforced phase and the matrix leads to the increase of dislocation density in the composite [21]. The hardness of the composite was improved. (2) The addition of the reinforcing phase effectively hinders the dislocation movement in the matrix and improves the deformation resistance of the material. (3) Graphene and SiC have greater hardness [22], which is endowed to the matrix due to load transfer [23]. The hardness value increases with the increase of the proportion of composite powder, which is due to the increase of the proportion of SiC nanoparticles, resulting in a continuous increase in hardness.

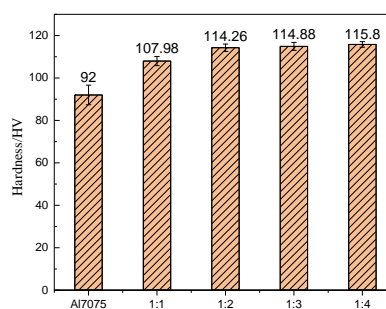


Fig. 8. Vickers hardness of aluminum matrix composites containing different ratios of composite Powders.

The tensile properties of the composite samples are shown in Fig. 9. Fig. 9a shows the engineering stress-strain curve of aluminum matrix composites with different ratios of composite powders. The curve has four typical stages: (1) elastic loading stage, which lasts until the material reaches the yield point, (2) substantial strain hardening, (3) "stable" state, and the flow stress is almost unchanged. The residual deformation is close to the peak stress. (4) after reaching the peak stress, the residual deformation continues to elongate until the final fracture [23,24]. Fig. 9b shows ultimate tensile strength (UTS) and post-break elongation (δ) of aluminum matrix composites with different ratios of composite powders. It can be seen from the diagram that, compared with the matrix material, the ultimate tensile strength and elongation at break of the composite were improved. With the increase of the ratio of composite powder, the UTS of the composite increases at first and then decreases and stabilizes at 320-330 MPa. The composite first increased and stabilized at about 6%, and decreased rapidly when the ratio of composite powder was 1: 4. When the ratio of composite powder is 1: 1, the UTS of the composite reaches the maximum value, which is 373.59MPa. Compared with the matrix, it increased by 44.63%. However, when the ratio of composite powder in the composite is 1: 4, the UTS and A of the composite were smaller than that of the composite with the ratio of 1:1. This is mainly due to the following reasons: (1) due to the addition of a large number of SiC nanoparticles during ball milling, the structure of graphene is destroyed, which can be confirmed in Fig. 4; (2) because a large number of SiC nanoparticles are located at the boundary of Al grains, cracks are preferentially formed in SiC nanoparticles and extended to Al matrix during tension, which reduces the tensile properties of the composites. Fig. 9c shows the strengthening incremental of reinforcements in aluminum matrix composites. The formula used is $R=(\sigma_c-\sigma_m)/\sigma_m$ [16], where σ_c and σ_m represent the UTS of the reinforced composite and matrix, respectively. The results in Fig. 9c show that the strengthening ability of the composite reinforced phase prepared in this paper is higher than that of the Ref. [25-29]. This indicates that the composite reinforced phase has a good application prospect in aluminum matrix composites.

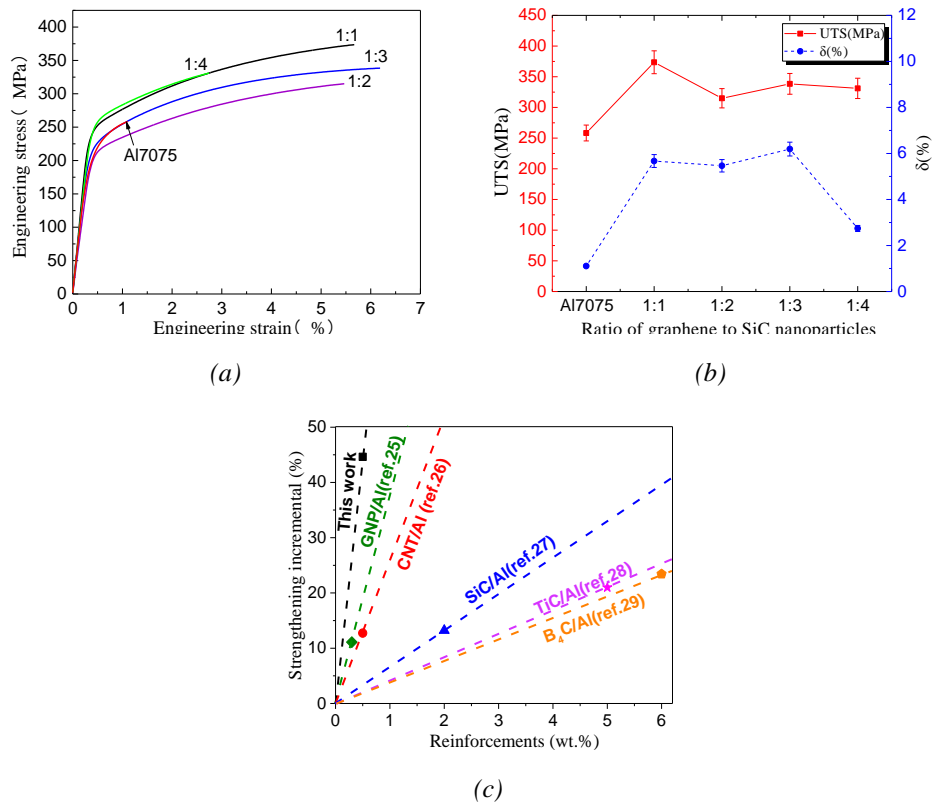


Fig. 9. The tensile properties of the composite samples, (a) Engineering stress- strain curve,(b) Ultimate tensile strength and elongation,(c) Strengthening incremental of reinforcements.

Fig. 10 shows the tensile fracture micrographs of aluminum matrix composites containing different ratios of composite powders. It can be found that with the increase of the ratio, the dimples in the tensile fracture micrographs of the composites become less and less. The torn ridge also gradually smoothed out, or even disappeared. This shows that the fracture mechanism of the composites changes from toughness to brittleness with the increase of the ratio of the two reinforced phases.

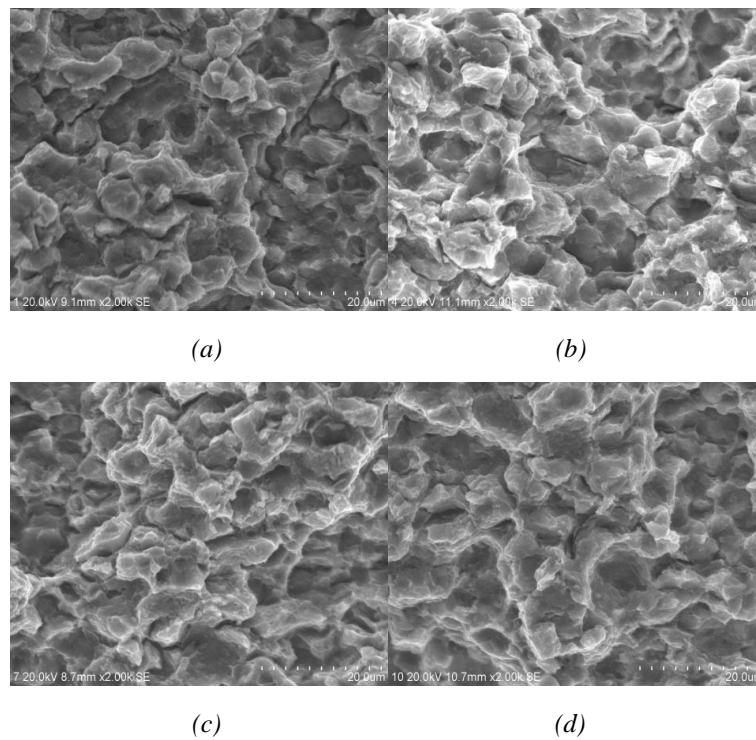


Fig. 10. Tensile fracture micrographs of aluminum matrix composites containing different ratios of composite powders (a)1:1,(b)1:2,(c)1:3,(d)1:4.

4. Conclusions

In this paper, SiC nanoparticles coated by graphene were prepared by high energy ball milling, and then aluminum matrix composites were prepared by secondary ball milling and vacuum hot pressing sintering. The enhancement effect of the two reinforcement phases under different ratios were investigated. The results show that the microstructure of graphene is destroyed with the increase of the composite ratio of the two reinforcing phases. The composite reinforced phase with good coating content was found for the ratio of 1:1 of graphene vs SiC nanoparticle.

The composite reinforced phase was mainly distributed at the Al grain boundaries. SiC nanoparticles were wrapped in graphene. The aluminum carbide was not found on the interfaces between the reinforced phase and the matrix. The tensile test results show that the UTS of the composite reaches the maximum when the ratio of the two reinforced phases is 1:1. The strength improvement of this composite reinforced phase is higher than that of other reinforcement phases. Moreover, the fracture mechanism of the composites changed from toughness to brittleness with the increase of the ratios of the two reinforced phases.

Acknowledgements

This work was supported by Shenyang Young and Middle-aged Science and Technology Innovation Talents Project (RC180214) in Liaoning Province, China and the Program for Guangdong Introducing Innovative and Entrepreneurial Teams (NO: 2016ZT06G025).

References

- [1] M. O. Bodunrin, K. K. Alaneme, L. H. Chown, *Journal of materials research and technology* **4**(4), 434 (2015).
- [2] J. H. Liu, U. Khan, J. Coleman, B. Fernandez, P. Rodriguez, S. Naher, D. Brabazon, *Materials & design* **94**, 87 (2016).
- [3] G. Pandi, S. Muthusamy, *Procedia engineering* **38**, 1399 (2012).
- [4] P. Pradeep, P. S. S. R. Kumar, S. Jayabal, *International Journal of Civil Engineering and Technology (IJCIET)* **8**(9), 178 (2017).
- [5] A. V. Muley, S. Aravindan, I. P. Singh, *Manufacturing Review* **2**, 15 (2015).
- [6] S. N. Alam, L. Kumar, *Materials Science and Engineering: A* **667**, 16 (2016).
- [7] A. K. Geim, K. S. Novoselov, *Nature materials* **6**(3), 183 (2007).
- [8] C. Lee, X. Wei, J. W. Kysar, W. Jeffrey, *Science* **321**(5887), 385 (2008).
- [9] M. E. Turan, *Journal of Alloys and Compounds* **788**, 352 (2019).
- [10] J. Li, X. Zhang, L. Geng, *Materials & Design* **144**, 159 (2018).
- [11] A. Bisht, M. Srivastava, R. M. Kumar, I. Lahiri, D. Lahiri, *Materials Science and Engineering: A* **695**, 20 (2017).
- [12] P. B. Prakash, K. B. Raju, K. V. Subbaiah, N. M. Kandan, *Materials Today: Proceedings* **5**(6), 14281 (2018).
- [13] A. Smirnov, P. Peretyagin, J. F. Bartolomé, *Journal of the European Ceramic Society* **39**(12), 3491 (2019).
- [14] X. Wang, J. Zhao, E. Cui, H. Liu, Y. H. Dong, Z. F. Sun, *Ceramics International* **45**(17), 23384 (2019).
- [15] X. Gao, H. Yue, E. Guo, H. Zhang, X. Y. Lin, L. H. Yao, B. Wang, *Materials & Design* **94**, 54 (2016).
- [16] R. Pérez-Bustamante, D. Bolaños-Morales, J. Bonilla-Martínez, I. Estrada-Guel, R. Martínez-Sánchez, *Journal of alloys and compounds* **615**, S578 (2014).
- [17] A. Sharma, D. Narsimhachary, V. M. Sharma, I. Estrada-Guel, R. Martínez-Sánchez, *Surface and Coatings Technology* **368**, 175 (2019).
- [18] S. E. Shin, Y. J. Ko, D. H. Bae, *Composites Part B: Engineering* **106**, 66 (2016).
- [19] H. Zhang, C. Xu, W. Xiao, K. Ameyama, C. Ma, *Materials Science and Engineering: A* **658**, 8 (2016).
- [20] R. Pérez-Bustamante, F. Pérez-Bustamante, I. Estrada-Guel, L. Licea-Jiménez, M. Miki-Yoshida, R. Martínez-Sánchez, *Materials Characterization* **75**, 13 (2013).
- [21] M. R. Akbarpour, S. Alipour, A. Safarzadeh, H. S. Kim, *Composites Part B* **158**, 92 (2019).
- [22] X. M. Du, K. F. Zheng, T. Zhao, F. G. Liu, *Digest Journal of Nanomaterials and Biostructures* **13**(4), 1133 (2018).

- [23] X. M. Du, K. F. Zheng, F. G. Liu, Digest Journal of Nanomaterials and Biostructures **13**(1), 253-018).
- [24] H. Yue, L. Yao, X. Gao, S. Zhang, E. Guo, H. Zhang, X. Lin, B. Wang, Journal of Alloys and Compounds **691**, 755 (2017).
- [25] M. Rashad, F. Pan, A. Tang, A. Muhammad, Progress in Natural Science: Materials International **24**(2), 101 (2014).
- [26] J. Liao, M. J. Tan, I. Sridhar, Materials & Design **31**, S96 (2010).
- [27] Y. Yang, J. Lan, X. Li, Materials Science and Engineering: A **380**(1-2), 378 (2004).
- [28] K. J. Lijay, J. D. R. Selvam, I. Dinaharan, S. J. VIJAY, Transactions of Nonferrous Metals Society of China **26**(7), 1791 (2016).
- [29] M. Karnam, A. Shivaramakrishna, R. Joshi, T. H. Manjunatha, K. Veerabhadrappe, Materials Today: Proceedings **5**(11), 25102 (2018).